EUROPEAN ORGANIZATION FOR NUCLEAR RESEARCH

CERN/ISRC/69-12
14 March, 1969

INTERSECTING STORAGE RINGS COMMITTEE

PROPOSAL FOR AN EXPERIMENT ON THE ISR

MEASUREMENT OF THE p-p TOTAL CROSS SECTION

G. Bellettini, P.L. Braccini, C. Bradaschia, R.R. Castaldi, C. Cerri,
T. Del Prete, L. Foà, A. Menzione, G. Sanguinetti

Istituto di Fisica, PISA

Scuola Normale Superiore di PISA

Istituto Nazionale di Fisica Nucleare,
Sezione di PISA.

EUROPEAN ORGANIZATION FOR NUCLEAR RESEARCH

Proposal for an experiment on the ISR

MEASUREMENT OF THE p-p TOTAL CROSS-SECTION

G. Bellettini, P.L. Braccini, C. Bradaschia,
R. Castaldi, C. Cerri, T. Del Prete, L. Foà,
A. Menzione, G. Sanguinetti and M. Valdata

Istituto di Fisica dell'Università di Pisa
Scuola Normale Superiore, Pisa
Istituto Nazionale di Fisica Nucleare, Sezione di Pisa

Geneva - 10 March 1969

INTRODUCTION

One of the basic parameters to be measured at the ISR is the p-p total cross-section, σ_t. By stacking in the ISR two equally energetic beams between 10 and 28 GeV/c, σ_t can be measured between w = 20 and w = 56 GeV (w = total c.m.s. energy), corresponding to $\sim$ 200 and $\sim$ 1800 GeV/c incident momentum for a conventional machine. This would allow the result to be compared with the one that will be obtained at the forthcoming American 200 GeV proton accelerator, and also to extend the measurement at much higher energies.

If injection from the PS at energies below the transition in the accelerator cycle ($\sim$ 6 GeV) would be possible, data at an equivalent energy for a conventional machine of 60 GeV and below would also be obtained. This would allow a direct comparison to be made with data obtained at Serpukhov.

Cosmic-ray experiments have shown that $\sigma_t \neq 0$ [and of the order of 40 mb [1)]] at 10^3-10^4 GeV. On the other hand, extrapolation from present-day accelerator energies up to w = 56 GeV is subject to large uncertainties. A Regge-pole fit to all hadron total cross-sections, assuming the existence of a Pomeranchuk trajectory with $\alpha_p(0) = 1$ [2)], predicts $\sigma_t = 35.7$ mb at $w = \infty$, and $\sigma_t \sim 38$ mb at ISR energies. A Regge-pole model by Cabibbo et al. [3)], without a Pomeranchuk trajectory with $\alpha_p(0) = 1$, fits also well enough the data below 30 GeV, but predicts zero for the asymptotic cross-sections. A model by Frautschi and Margolis[4)] in which the p-p interaction is described as being due to single and multiple Pomeranchuk exchange, predicts an increasing total cross-section above 30 GeV/c. A comparison of the predictions of these models is shown in Fig. 1 for laboratory momenta below 1000 GeV/c. The difference between the various predictions ranges between 5 and 20 mb at ISR energies.

It is well known that p-p and $\bar{p}$-p total cross-section data can be used to check causality by comparing the dispersion relation predictions with the measured real part of the forward p-p elastic scattering amplitude [Re f (0)]. Such a comparison was made below 30 GeV [5)], and a satisfactory agreement was found within the theoretical uncertainties. Since Coulomb interference experiments are feasible also at the ISR [6)],

Re f(0) will be deduced from such data if σ_t is known. Within the uncertainty due to the lack of knowledge of the $\bar{p}$-p total cross-section, it will thus be possible to check dispersion relations predictions up to w = 56 GeV.

1.1 The experiment

The schematic layout of the experiment is shown in Fig. 2. Two (a and b) symmetrical counter hodoscope systems, H_1, H_2, S, H_3, H_4, detect charged particles emitted around the beam pipes, downstream from the interaction region. In both sections a and b, the coincidence (H_1H_2) covers the large-angle region, from 70 to 500 mrad, and the coincidence (H_3H_4) covers the small-angle region, from 9 to 80 mrad. Hodoscope S is used in the logic as a part of H_1. A counter hodoscope L covers the large-angle region over about 10% of the azimuthal angle.

A p-p collision is defined as a coincidence between one or more signals in the a-hodoscopes and one or more signals in the b-hodoscopes (trigger). Calculations show (see below) that at least $\sim$ 90% of the events should be detected in this way (this number increasing to $\sim$ 96% if pipes of 5 cm diameter are used).

In a fraction of cases, when a trigger occurs the contents of all hodoscopes are transferred into the memory of an on-line computer. From the angular distributions obtained for these events, the losses of the trigger system can be calculated (see Section 2.1).

A counter and spark chamber monitor system (M^a, M^b, M^0 in Fig. 2), placed on the horizontal plane, scans the longitudinal and vertical distributions of radiation centres around the interaction region. Such distributions provide at the same time the effective height of the interaction region h_{eff} which is needed to calculate the luminosity, and a relative monitor for the intensity of each of the two beams times the density of the residual gas (see Section 2.3).

Due to the request of an (ab) coincidence to define an event, the background from beam-gas interactions is expected to be negligibly small. However, such a background can be measured by displacing the two beams one with respect to the other in the vertical plane, in order to reduce the interaction volume to zero.

The proposed experiment is based on the following assumptions concerning the machine:

1) The experiment is installed on an even numbered interaction region.

2) The vacuum pipes are cylindrical, 13 cm in diameter, with thin ($\lesssim$ 0.5 mm steel) walls. Such pipes would not limit the ISR acceptance in the initial period of operation of the machine[7].

3) The residual gas in the interaction region is hydrogen with 5×10^{-11} torr pressure. This seems to be a reasonable assumption for the first period of operation of the ISR[7].

4) The two beams have a 1×6 cm^2 section (roughly rectangular, 1 cm in the vertical, 6 cm in the horizontal direction).

5) The two beams contain $N_1 = N_2 = 4 \times 10^{14}$ circulating protons. Background and accidental rates have been calculated under this assumption. The data collection rate is very high in this experiment, and from this point of view no strict requirement is made on the intensity of the beams.

On the above points the following comments should be made:

1) Use of an odd numbered interaction region would <u>not</u> make the experiment impossible, but would reduce its precision since larger solid angles around the beam axis would not be covered by the detectors.

2) Use of cylindrical pipes 5 cm in diameter would be welcome, since the fraction of detected interactions would increase from $\sim$ 90% to $\sim$ 96% (these estimates are discussed below). Pipes of such a section can be used if the machine is run in the Terwilliger scheme[7]. One may envisage running most of the experiment with 13 cm diameter pipes; doing a run with narrow pipes and with the Terwilliger scheme at the end in order to improve the extrapolation to zero loss in the beam holes. Although the use of flared pipes would be useful to reduce the interactions of small-angle secondaries in the walls, this complication does not seem to be necessary.

3) There is some safety on the tolerable vacuum, since at 5×10^{11} Torr (H_2) the background from beam-gas interactions is calculated to be small everywhere.

4) In addition to what is discussed in point (2) above, it appears that running the machine in the Terwilliger scheme would be interesting, because one could trigger only when the detected prongs come from a small region around the crossing point. A better rejection against beam-gas triggers would thus be obtained. However, to be able to impose such a constraint in the trigger, each hodoscope should be equipped with θ-planes (as discussed in Section 1.2 below), and the width of the θ-bins should be reduced. Such a complication seems unnecessary as far as the σ_t- measurement is concerned, since the triggering rate from beam-gas interactions is estimated to be small even with the proposed set-up. On the other hand, the possibility of running the ISR in the Terwilliger scheme and of modifying the detectors in order to define particle trajectories with a better precision should be kept in mind, because in this way one may be able to distinguish the elastic scattering events and one would learn more about the angular distribution of prongs in the complex events.

1.2 The hodoscope system

H_2 is a θ,ϕ hodoscope (whose planes will be named $H_2\theta$ and $H_2\phi$ in the following) centred around the downstream beam line at 2 m for the interaction region (i.r.) centre. Its geometry is best understood by an inspection of Fig. 3. In coincidence with H_1 or with counter S, it covers an angular region $70 \lesssim \theta \lesssim 500$ mrad, and $0 < \phi < 2\pi$, with the exception of the hole which is needed to let the second tube pass. Both θ- and ϕ-planes are split into eight parts. H_1 is a similar ϕ-hodoscope placed at 100 cm from the i.r. centre (also sketched in Fig. 3). It is split into eight elements, which are rotated by $2\pi/16$ with respect to the elements of $H_2\phi$. Together with $H_2\phi$, it allows the splitting of the ϕ-interval into 16 parts.

Hodoscopes H_3 and H_4 are similar to H_1,H_2, and cover the solid angle $0 < \phi < 2\pi$, $9 \lesssim \theta \lesssim 80$ mrad. The dimensions of the elements

of $H_2\theta$, $H_4\theta$ and the fluxes of useful particles through each of them (calculated as explained in Section 2.2 below) are listed in Table 1.

We have considered the opportunity of adding θ-defining planes also in H_1 and H_3 and using them in the trigger. However, if a rather large width were chosen for these elements, similar to the ones listed in Table 1 for H_2 and H_4, the section of beam lines viewed by any of the θ-defining elements in H_4 in coincidence with the corresponding θ-element in H_3 would be almost the same as in coincidence with the full H_3. Therefore splitting H_3 into θ-bins would not sensibly reduce the background of direct tracks from beam-gas interactions. Since the area of H_3 is small, the accidental coincidence rate is also expected to be unimportant (see Section 2.4). Similar arguments lead one to conclude that no splitting of H_1 in θ-bins is necessary.

Counter S is logically an element of H_1. Without it, the size of H_3,H_4 would have to be substantially increased.

1.3 The electronic logic

A scheme of the logic of the electronics, showing how a coincidence between two adjacent hodoscopes (H_3 and H_4, as an example) is obtained, is given in Fig. 4. Four such electronic systems are actually used to generate a trigger.

ϕ-bins of $H_4\phi$ are set in coincidence with the two bins of H_3 facing them. This system, together with the wide radial dimensions of H_3, ensure a particle emitted by the target and crossing $H_4\phi$, to be always detected by one of these coincidences.

After this filtering, signals from $H_4\phi$ are fed to four OR-circuits to give a signal for a particle crossing any of the corresponding four quadrants in $H_4\theta$. These signals are strobed to open gates on patterns.

The strobe pulse is generated by the coincidence $\left[(H_1^a, H_2^a\phi) \text{ OR } (H_3^a, H_4^a\phi)\right]$ AND $\left[(H_1^b, H_2^b\phi) \text{ OR } (H_3^b, H_4^b\phi)\right]$. The content of the θ-bins in the $H_2\theta$, $H_4\theta$ quadrants is recorded in the patterns, together with the content of the particular bins that have been used in generating the gating pulse of each pattern.

The patterns are provided with output OR-circuits which are used to generate a signal if any of the θ-bins of the a-channel have been fired. Coincidence of this signal with an analogous one from channel b ("TRIGGER") indicates that a good event occurred and is counted on a scaler. The trigger also starts the transfer procedure of the content of the patterns to an on-line computer. It is expected that only a rather small fraction of events will be needed for computer analysis of the angular distribution of the secondaries. The gating-inhibit logic of the electronics is not indicated in Fig. 4 and will not be discussed here.

2.1 Data reduction and calculation of the total cross-section

The rate of p-p interactions lost by the trigger can be calculated from the θ-distributions of the events that show one single particle in branch a(b) [and any multiplicity in branch b(a)] of the system. Such distributions are obtained on-line from the sample of the data analysed by the computer.

Let N_0 be the σ_T-scaler reading, N_c the number of events transferred to the computer, and N^{1a} the number of such events showing a single track in the a-section. The partial cross-section $dN^{1a}/d\Omega_a$ can be extrapolated from the covered solid angle to the full a hemisphere. The loss of events through the holes in the counters (n^{1a}_{hole} and n'^{1a}_{hole}) or at large angles (n^{1a}_{out}) can then be calculated. The precision with which such an extrapolation can be made depends from the actual loss of events due to the limited solid angle covered. This point is discussed in some detail in Section 2.2. By a similar extrapolation of $dN^{1b}/d\Omega_b$ the loss of the events of "1b" type can also be calculated.

Let N^{11} be the number of events (amongst the N_c events transferred to the computer) showing one track in the a-section and one track in the b-section. By extrapolation of the distribution $d^2N^{11}/d\Omega_a\, d\Omega_b$ over θ_a and θ_b, the losses of the zero-zero type (n^{00}) can also be calculated. N_c should therefore be corrected by the following amount:

$$N_{c,true} = N_c + n^{1a}_{hole} + n'^{1a}_{hole} + n^{1a}_{out} + n^{1b}_{hole} + n'^{1b}_{hole} + n^{1b}_{out} + n^{00} = N_c + \Delta N_c \,.$$

The events of type 1a, 1b, 11, contain events from any multiplicity, for which all but one prong in one or both sections escaped detection. Therefore one may state that the correction for loss of these events is the only one to be applied. Thus the correct number to be used in the calculation of the total cross-section is

$$N_{0,true} = N_0\left(1 + \frac{\Delta N_c}{N_c}\right) .$$

2.2 Estimated efficiency

The main processes contributing losses to the (ab) trigger may be schematized as follows:

a) elastic scattering events inside the beam pipe;

b) N^* excitation events in processes such as $pp \rightarrow pN^*$ or $pp \rightarrow N^*N^*$, with isobars decaying without any charged secondary within the useful solid angle in section a or b;

c) strongly inelastic events, such as $pp \rightarrow pN^* + n\pi$ without a charged secondary within the useful solid angle in section a or b.

Estimates of such losses are given in the following. Losses have been assumed to be caused mainly by the central hole in hodoscopes H_3, H_4, and by the finite radial dimensions of hodoscopes H_1, H_2. The losses through the off-central hole in H_1, H_2 have been calculated to be negligible.

a) Loss of elastic scattering events

Under the following assumptions for the elastic scattering cross-section

$$d\sigma_{el}/dt \propto e^{bt} , \qquad b = 10\ (GeV/c)^{-2} ,$$

the following estimates for the relative loss ($\Delta R/R$) were obtained:

$$13 \text{ cm diameter pipes: } \frac{\Delta R}{R} \approx 25\%$$

$$5 \text{ cm diameter pipes: } \frac{\Delta R}{R} \sim 6\% .$$

These losses are all due to the central holes.

b) Loss of isobar excitation events

A typical value of 1690 MeV was chosen for the isobar mass. The losses were calculated only for single isobar excitation events, $pp \to pN^*$, but the result can be taken to represent also a pessimistic estimate of the loss of double isobar excitation events, $pp \to N^*N^*$, since in the reaction $pp \to pN^*$ the proton in the final state has a larger probability of escaping detection than does the N^* itself.

The following assumptions were made on the production and decay mechanism:

1) Production cross-section, $d\sigma/dt \propto e^{bt}$, with $b = 10$ $(GeV/c)^{-2}$. This is a pessimistic assumption, since most of the isobars [the only known exception being the $N^*(1470)$] appear to be produced with $b \sim 5$ $(GeV/c)^{-2}$, and since with increasing b the final-state proton has an increasing probability of escaping detection (through the central hole). The detection probability of the N^* does not depend appreciably on b.

2) Isobar decay channels, π^+-n and π^0-p only, in the ratio 2:1 (as for an isospin ½ state). Since the probability for the isobar escaping detection is larger for a two-body decay than for a decay into more bodies, this assumption tends to produce a pessimistic estimate of the loss.

The following estimates for the relative losses were obtained:

13 cm diameter pipes: $\frac{\Delta R}{R} \sim 27\%$

(2.5% loss of the isobar, mostly at large angles, 24.5% loss of the proton in the central holes).

5 cm diameter pipes: $\frac{\Delta R}{p} \sim 8\%$

($\sim$ 2.0% isobar loss, and $\sim$ 6% proton loss).

c) Loss of more complicated inelastic events

The loss of these events was calculated by making use of the Hagedorn and Ranft (HR) thermodynamical model[8] and also checked with a simple intuitive model of high-energy inelastic events.

The average multiplicity of charged prongs in p-p interactions at w = 50 GeV is approximately $\bar{n} = 14$ [1]. In the thermodynamical model, the multiplicity distribution of events can be taken to be a Poisson distribution

$$f(n) = \frac{\bar{n}^{n}}{n!} e^{-\bar{n}} . \qquad (1)$$

Based on information from cosmic-ray events, the assumption was made that each event could be built up by two cascades with axes along the directions of the incident protons. The multiplicities were assumed to be distributed according to Eq. (1), with $\bar{n} = 7$. This is consistent with an over-all Poisson multiplicity distribution with $\bar{n} = 14$.

The probability for an interaction to be detected was calculated as the probability for each of the two cascades to give (independently from each other) at least one charged prong in the associated hodoscopes. To find the probability for each cascade to be detected in the associated hodoscopes (P_{in}), the momentum spectra of long-lived charged secondaries from inelastic events, as predicted at w = 50 GeV in the HR model, were calculated in the ISR reference frame[9]. Such spectra were integrated over momentum, and a cross-section for emission of a charged secondary as a function of the angle with respect to the beam axis between 0° and 90° was obtained. Such a cross-section is shown in Fig. 5. By integrating this cross-section over the useful solid angle, the result $P_{in} \approx 0.58$ was found, independent of the size of the holes in the hodoscopes.

Under the assumption that for any multiplicity the average probability for one prong to be detected is P_{in}, the detection efficiency for each of the two cascades and the over-all trigger efficiency can be calculated as an average over the multiplicity distribution.

For very low multiplicity events (for example, $n \lesssim 2$) this assumption is not really justified. However, one should remember that for a Poisson distribution with $\bar{n} = 7$, events with $n \lesssim 2$ have a very low probability. For the same reason, the problem of double-counting of low multiplicity events, which is raised by having treated elastic and isobar excitation events separately, is of no practical importance.

The probability for losing one prong is

$$P_{out} = 1 - P_{in} = 0.42$$

and the probability of losing one cascade of multiplicity n is P_{out}^{n}. As an average over Eq. (1), with $\bar{n} = 7$, one obtains for the relative loss in each hemisphere

$$\frac{\Delta R}{R} = 1.7\% \ .$$

Since the (ab) coincidence is required in the trigger, the over-all loss of events of this category is therefore estimated to be

$$\frac{\Delta R}{R} \sim 3.5\% \ .$$

Whilst the above estimate is in our opinion very reasonable, an attempt was also made to estimate a possible upper limit for the loss of very inelastic events. The scheme adopted was as follows. All events were assumed to be of the type

$$pp \rightarrow \text{leading baryons} + \text{pion fireball} = pN^{*} + n\pi \ ,$$

the leading baryons and the pion fireball being produced independently from each other. The production angular distribution of the baryons was assumed to be the same as for single isobar excitation events. Consequently, their detection probability was calculated as in point (b) above. The pion fireball was assumed to be produced at rest in the ISR reference frame, and to decay isotropically according to Eq. (1) with $\bar{n} = 12$.

It appears that such assumptions should produce a pessimistic estimate of the loss. As the leading baryon is assumed to be strongly collimated in the forward direction, a very large loss is produced through the beam holes. This is even more true, because one such baryon is assumed to be unexcited. The fireball pions being assumed to be emitted isotropically, a large loss is produced also at large angles.

The calculation of the over-all probability in order to obtain a trigger for such events is somewhat delicate, due to the many configurations possible. As an average over multiplicities, the loss is found to be

$$\text{13 cm diameter hole} \qquad \frac{\Delta R}{R} \simeq 11\%$$

$$\text{5 cm diameter hole} \qquad \frac{\Delta R}{R} \sim 3\% \ .$$

In view of the pessimistic assumptions made, this result -- although less favourable than the result obtained from the HR model calculation -- looks rather encouraging.

The over-all loss depends on the partial cross-sections for events of categories (a), (b) and (c). One may assume σ_t = 38 mb, and

$$\begin{aligned} \sigma(pp \to pp) &= 9 \text{ mb} \\ \sigma(pp \to pN^*) &= 2 \text{ mb} \\ \sigma(\text{very inelastic}) &= 27 \text{ mb} \end{aligned}$$

roughly as at 30 GeV laboratory momentum. The estimated over-all loss is, in this case, according to the HR model:

$$\text{13 cm diameter holes:} \quad \Delta\sigma_t \sim 3.5 \text{ mb}, \quad \frac{\Delta\sigma_t}{\sigma_t} \sim 10\%$$

$$\text{5 cm diameter holes:} \quad \Delta\sigma_t \sim 1.5 \text{ mb}, \quad \frac{\Delta\sigma_t}{\sigma_t} \sim 4\% \ .$$

The contribution to these losses from the beam holes and at large angles are listed in Table 2. Qualitatively, one may observe that with pipes of 13 cm diameter, the loss is expected to be mostly due to the beam holes, whilst with 5 cm diameter pipes the losses are roughly equally shared between small and large angles.

2.3 The monitor

The cross-section σ can be calculated from the measured rate

$$R = L\sigma$$

provided the luminosity L is known:

$$L = c \frac{N_a N_b}{(2\pi R)^2} \frac{1}{h_{eff} \operatorname{tg} \frac{\alpha}{2}}$$

(N_a, N_b = numbers of stacked protons in the two rings, α = crossing angle, R = average ring radius). The essential parameter to be measured in this expression is h_{eff}, which is the effective height of the overlap region.

Systems to measure this parameter have been proposed by several authors[10]. In terms of the arbitrarily normalized particle distributions in the two beams at the crossing point, $\rho_a(z)$ and $\rho_b(z)$ ($z \equiv$ vertical coordinate, normal to the plane containing the beams), the quantity $1/h_{eff}$ can be expressed as

$$\frac{1}{h_{eff}} = - \frac{\int \rho^a(z)\rho^b(z)\, dz}{\int \rho^a(z)\, dz \int \rho^b(z)\, dz}$$

The proposed monitor system comprises three spark chamber and counter telescopes M^a, M^b and M^0, as sketched in Figs. 2 and 3. Small-angle telescopes M^a and M^b (Fig. 6) are identical to each other. These telescopes measure the z-distribution of the radiation centres produced in the beam-gas interactions over a path four metres long, extending from three to seven metres, upstream from the interaction region. The coincidence (C_1C_2) is used as a trigger for spark chambers SC_1 and SC_2. Thus mostly tracks originating from the a(b) beam are accepted in $M^a(M^b)$. Contamination from the other beam is estimated to be negligible.

Since the vertical beam divergence in the intersecting region is $\approx \pm 0.5$ mrad [11], some correction should be applied to obtain $\rho^a[\rho^b(z)]$ at the crossing point, as explained below. The system as a whole has been planned in such a way as to allow an over-all z-resolution better than 1 mm. The main parameters determining this resolution are: (a) the distance (d_1) of SC_1 from the beam axis; (b) the distance from the beam axis (d_2) of the particle trajectory at the SC_2 position; (c) the dip angle (ϕ) of the particle trajectory on the horizontal plane; (d) the space resolution ($\delta z_1, \delta z_2$)

of SC_1 and SC_2. The effect of multiple scattering in the pipe walls is not very important, as long as the wall thickness ($\lesssim$ 0.5 steel) and distance d_1 ($\sim$ 20 cm, see below) are small.

With the following values for the quantities discussed above: d_1 = 20 cm, 50 cm < d_2 < 150 cm, ϕ < 0.02 rad, δz_1, δz_2 = 0.3 mm, and for a 6 cm horizontal beam width, the over-all z-resolution was calculated to be $\lesssim$ 1 mm FWHM. Such a resolution seems good enough, since the $\rho^{a,b}(z)$ distributions are expected to be $\gtrsim$ 1 cm wide.

The useful rate in $M^{a,b}$ depends on the solid angle, as defined by C_2. For $N_{a,b} = 4 \times 10^{14}$ protons, 5×10^{-11} Torr residual gas (H_2) pressure, and for the geometry discussed above, this rate was calculated by making use of the Cocconi, Koester and Perkins (CKP) empirical formula to fit the production spectra of charged secondaries in p-p collisions[12]. The CKP formula was integrated over momentum, and over the solid angle accepted by the (C_1C_2) coincidence as a function of the longitudinal coordinate along the beam (hereafter called x). The result is:

$$R^{a,b} \sim 30 \text{ sec}^{-1} .$$

Such a rate is enough to measure $\rho^{a,b}(z)$ with a very good statistical accuracy over a time of a few minutes. During this time the luminosity is expected to be sensibly constant.

The background flux through SC_1 and SC_2 was also calculated in a similar way. The flux through SC_1, which was assumed to be 5 cm high and 400 cm long, was calculated to be $\sim$ 500 sec^{-1}. The flux through SC_2 (6 cm high and 100 cm long) was found to be mostly due to the nearest beam, and to be only a few times larger than $R^{a,b}$. These rates are small and well tolerated by the chambers.

As only a measurement of the vertical coordinate is needed at the SC_1 position, a wire spark chamber with only horizontal wires can be used. By splitting it into four 1-metre long chambers, four independent measurements of $\rho^{a,b}(z)$ would be obtained at x $\sim$ 3.5, 4.5, 5.5, and 6.5 metres from the crossing point. An extrapolation to calculate $\rho^{a,b}(z)$ at the crossing point will thus be possible.

Whilst data from M^a,M^b alone are, in principle, enough to calculate the luminosity, the result would be very sensitive to possible relative systematic errors in the absolute z-scale. Therefore, also the z-distribution of p-p interaction at the crossing point, which is proportional to $\rho^a(z)\rho^b(z)$, should be measured. Such measurement is performed by the large-angle spark chamber and counter telescope M^0, which is sketched in some detail in Fig. 7. Spark chambers SC_1 and SC_2 (110 and 160 cm wide, 5 and 10 cm high, respectively), are triggered by the (C_1C_2) coincidence. In this way particles coming from the beam area are selected. By making use of tracks emitted over a constant solid angle ($\Delta\theta \sim 2 \times 10^{-2}$ sr), a proportional x,z scan of the density of radiation centres in the area around the interaction region is made. This density is expected to be very strong inside the two beam-overlap region (due to beam-beam interactions) and very weak outside (beam-gas interactions).

The expected rate from p-p interactions was calculated with the HR model. A rough estimate of the rate from beam-gas interactions was obtained with the CKP formula. The results are as follows:

$$\frac{dN_{pp}}{d\Omega}\,\Delta\Omega \sim 1500\ \text{sec}^{-1}$$

$$\frac{dN_{p-gas}}{d\Omega}\,\Delta\Omega \sim 0.5\ \text{sec}^{-1}\ .$$

Although the CKP formula is very inaccurate at such large angles, the result shows that the background from beam-gas interactions should be negligible. However, since a wider x-region than the hot area is explored, this background is measured directly and can be subtracted. By integration over x of the x,z density function, the shape of the function $\rho^a(z)\ \rho^b(z)$ can be obtained.

The over-all spark chamber triggering rate is about

$$N_{trg} \approx 3\ N_{pp} \approx 4.5 \times 10^3\ \text{sec}^{-1}\ .$$

Therefore a very high statistical accuracy on the measurement of the $\rho^a(z)\ \rho^b(z)$ shape should be obtainable in an extremely short time.

The rate of background tracks in the chambers was estimated by suitably scaling the result by de Raad[13] of a flux of 1.5×10^4 particles cm^{-1} sec^{-1} on a ring normal to one of the circulating beams, when the residual gas pressure is 10^{-10} Torr of N_2. The result is

$$N_{bgd}\ (SC_1 + SC_2) \sim 3000\ sec^{-1}\ .$$

Such a rate is rather small, and can be well tolerated by the spark-chambers.

2.4 The background rate in the hodoscopes

By making use of the CKP formula, the flux of charged particles from beam-gas interactions, integrated over the beam path in the interaction region upstream from the hodoscope planes, is calculated to be of about 5×10^4 particles per second over the (H_3H_4) region (for $N_1 = N_2 = 4 \times 10^{14}$ protons and 5×10^{-11} Torr pressure of residual hydrogen gas, as usual). The situation is better for (H_1H_2). This gives a rate of accidental (ab) coincidences of $\sim$ 100 per second, which is much smaller than the expected rate of good events (about 10^5 per second). The physically correlated (ab) events with a second charged particle emitted backwards are expected to have a negligible rate.

Other sources of background, such as accidentals in the (H_3H_4) coincidences, are negligibly small.

2.5 Precision in the σ_t measurement

The precision attainable in the σ_t measurement can be estimated from the relationships

$$\sigma_t = \frac{R}{L}\ , \qquad L \propto \frac{1}{h_{eff}} = \frac{\int \rho^a \rho^b dz}{\int \rho^a dz \int \rho^b dz}\ .$$

Variables that presumably will be known with a precision better than 1% have not been indicated explicitly. Since the function $\rho^a(z)\rho^b(z)$ is measured by M^0 with very high statistical accuracy, one can further assume that

$$\frac{\Delta\sigma_t}{\sigma_t} \sim \sqrt{\left(\frac{\Delta R}{R}\right)^2 + 2\left(\frac{\delta \int\rho^{a,b}(z)dz}{\int\rho^{a,b}(z)dz}\right)^2}$$

In 10' time, about 10^4 events (see Section 2.3) and consequently a statistical accuracy of $\sim$ 1% on $\int\rho^{a,b}(z)dz$ can be obtained.

The error on the rate $\Delta R/R$ will be due to the limited accuracy attainable in the extrapolation procedure which was discussed in Section 2.2. To correct for losses in the beam holes, a sample of events is used comprising about 75% of all elastic scattering events, together with more complicated events. Elastic scattering events are collected by the system at a rate of $\sim 1.8 \times 10^4$ sec^{-1}. Therefore the angular distributions to be used in the extrapolation will be known to a very high accuracy. The correction to be made (see Table 2) corresponds to a rate of $\sim 7 \times 10^3$ sec^{-1}. In such a condition, one may safely assume that the required correction will be done with a precision better than 25%. This would imply an error smaller than 2% in the total cross-section. The situation would, of course, be much better with 5 cm diameter pipes.

The loss at $\theta > 30°$ being less important than the loss in the beam holes (Table 2), a smaller relative error or σ_t should be produced by the extrapolation to be made at large angles. In the isobar + pionization model which was discussed in Section 2.2, the frequency of events at $\theta \gtrsim 20°$ which are useful in such an extrapolation, was calculated to be $\sim$ 4500 sec^{-1}, corresponding to $\sim$ 4.5% of the collected events. Therefore also at large angles the statistical accuracy of the angular distributions to be used in the extrapolation should be very high. One may tentatively assume that also this extrapolation will be possible with an error smaller than 25%. This would produce an error smaller than 1% on σ_t (see Table 2).

By combining the errors on the luminosity and on the rate, one gets in this way

$$\frac{\Delta\sigma_t}{\sigma_t} \lesssim 3\% \ , \quad \Delta\sigma_t \lesssim 1 \text{ mb}.$$

The above estimate was obtained under the most conservative assumptions one could think of. It is also worth noticing that the error in the extrapolation at large angles would be reduced by making use of information from the large-angle hodoscope L (Fig. 2).

The error in the extrapolation at small angles would be qualitatively reduced by running with the Terwilliger scheme and 5 cm diameter pipes. Data from some independent experiment on small-angle scattering inside the beam pipes[6], may also be used to improve the extrapolation.

3. FINAL COMMENTS AND CONCLUSIONS

The proposed set-up is, to our belief, suited to measuring the total cross-section to within a few per cent. However, the experiment has been planned in such a way that an increase of the hodoscope elements to cover a larger solid angle would be easy, in case the loss of events should turn out to be important.

The hodoscope structure of the detectors, which was planned mainly to provide a selective trigger against background, can also be used to study some properties of high multiplicity events. Some information on the distribution of particles at large angles is given by hodoscope L (Fig. 2). If additional θ-defining planes were added to hodoscopes H_1 and H_3, an even more selective trigger logic would be possible, and more detailed information on the structure of the events would also be obtained. A measurement of the elastic differential cross-section would perhaps be possible as well.

Detection of photons and neutrons on the solid angle covered by H_3 would be rather easy, provided a suitable detector is substituted for H_3 and H_4. An exporatory run with such a detector may be interesting; for example, to measure the charge-exchange-like reactions that would not trigger the proposed set-up. Such cross-sections should, however, be extremely small.

No estimate of running time is made for this experiment. On the one hand, it appears rather arbitrary to make such an estimate now. On the other hand, this experiment has basically no problem of rate.

Table 1

Hodoscope	Bin	Int. diam.	Width	Useful flux
For 5 cm diameter pipe only	1	5 cm	2 cm	2.8×10^3 sec^{-1}
	2	9	2	3.6
$H_4\Theta$	3	13	2	4.4
	4	17	2	4.2
	5	21	2	4.2
	6	25	2	3.8
	7	29	2	3.3
	8	33	2.5	3.2
	9	38	3.5	2.7
	10	45	6.8	2.8
	11	58	8.5	2.4
	12	76	10.0	2.6
$H_2\Theta$	1	13 cm	5.0 cm	6.5×10^3 sec^{-1}
	2	23	8.5	11.5
	3	40	10.0	12.0
	4	60	10.0	10.0
	5	80	15.0	9.0
	6	110	15.0	7.5
	7	140	15.0	6.0
	8	170	20.0	8.0

Table 2

Diameter of beam pipes	Reaction channel	Cross-section σ_i	Loss inside the beam pipes $\Delta\sigma_i/\sigma_i$	Loss at large angles $\Delta\sigma_i/\sigma_i$	Over-all loss in the i-channel $\Delta\sigma_i/\sigma_t$	Over-all loss $\Delta\sigma_t/\sigma_t$
5 cm	a) pp→pp	9 mb	∿6%	∿0	∿1.4%	∿4%
	b) pp→pN*	2 mb	∿8%	∿0	∿0.4%	
	c) very inelastic	27 mb	∿0	∿3.5%	∿2.4%	
13 cm	a) pp→pp	9 mb	∿25%	∿0	∿6%	∿10%
	b) pp→pN*	2 mb	∿27%	∿0	∿1.4%	
	c) very inelastic	27 mb	∿0	∿3.5%	∿2.4%	

REFERENCES

1) N. Koshiba, Rapporteur's talk at the 10th Int. Conf. on Cosmic Rays, Calgary (1968).

2) V. Barger, Proc. Topical Conference on High-Energy Collisions of Hadrons, CERN 68-7 (1968).

3) N. Cabibbo, L. Horwitz, J.J. Kokkedee and Y. Ne'eman, Nuovo Cimento 45 A, 275 (1966).

4) S. Frautschi and B. Margolis, Nuovo Cimento 46 A, 1155 (1968).

5) K.J. Foley et al., Phys.Rev.Letters 19, 857 (1967).

6) L. di Lella, "Elastic proton-proton scattering with the ISR", Contributed paper at the ISR User's Meeting CERN 10-11 June 1968.
U. Amaldi, G. Matthiae and P. Strolin, "The measurement of proton-proton differential cross-section in the angular region of Coulomb scattering at the ISR", February 1969.

7) We are grateful to E. Fischer and P. Strolin for discussions on these points.

8) R. Hagedorn and J. Ranft, supplements to Nuovo Cimento 6, 169 (1968). We are grateful to Prof. R. Hagedorn for several useful discussions on the application of this model to our problem.

9) The computer program was kindly given to us by C. Daum.

10) P. Darriulat and C. Rubbia, "On beam monitoring for ISR experiments", 28 February 1968.
J. Steinberger, "Suggestions for a luminosity measurement for the ISR", June 1968.
W. Schnell, "A mechanical beam profile monitor for the ISR", June 1968.
A.P. Onuchin, NP internal report 68-26 (1968).

11) P. Strolin, internal report CERN-ISR-TH/68-36.

12) G. Cocconi, L.J. Koester and D.H. Perkins, UCRL 10022.

13) B. de Raad, "Beam-Gas Interactions in the ISR", CERN internal report PS/6487.

Figure captions

Fig. 1 : pp and $\bar{p}p$ total cross-sections up to 1000 GeV/c beam momentum, as predicted by Cabibbo et al.[3] (full curves), by Barger[2] (dotted curves) and by Frautschi and Margolis for p-p scattering[4] (shadowed area).

Fig. 2 : Layout of the experiment.

Fig. 3 : Drawing of the ISR interaction region with one arm of the hodoscope system.

Fig. 4 : Diagram of the electronics.

Fig. 5 : Angular distribution of single charged secondaries in the ISR reference frame, at w = 50 GeV, according to the H.L. thermodynamical model.

Fig. 6 : Sketch of the monitor telescope, $M^a(M^b)$. SC_1 and SC_2 are spark chambers. C_1 and C_2 are the trigger counters.

Fig. 7 : Sketch of the monitor telescope M^a. SC_1 and SC_2 are spark chambers. C_1 and C_2 are the trigger counters.

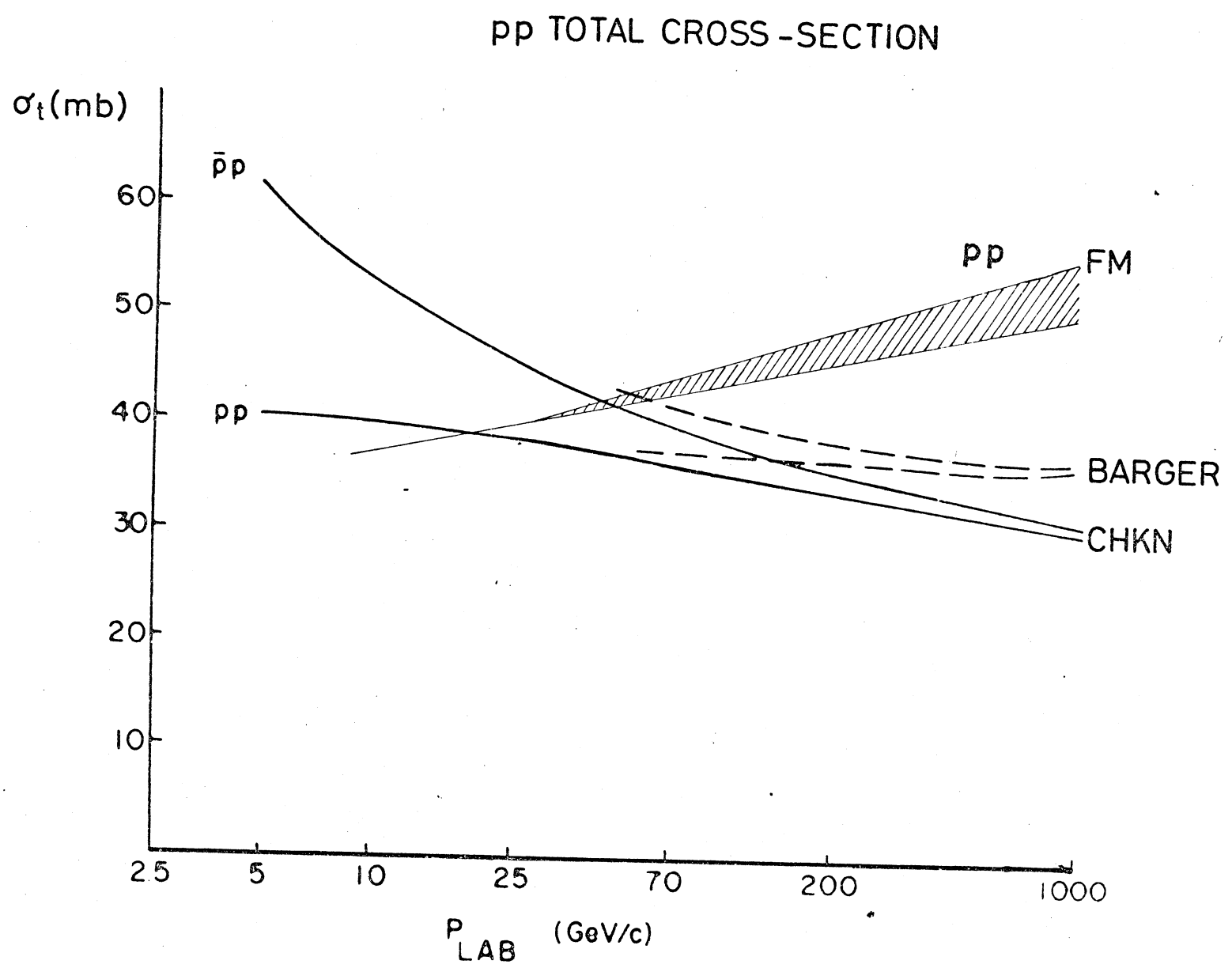
pp TOTAL CROSS-SECTION
σ_t(mb)
$\bar{p}p$
pp
FM
BARGER
CHKN
60
50
40
30
20
10
2.5
5
10
25
70
200
1000
P_{LAB} (GeV/c)

Fig. 1

GENERAL LAY-OUT OF THE EXPERIMENT

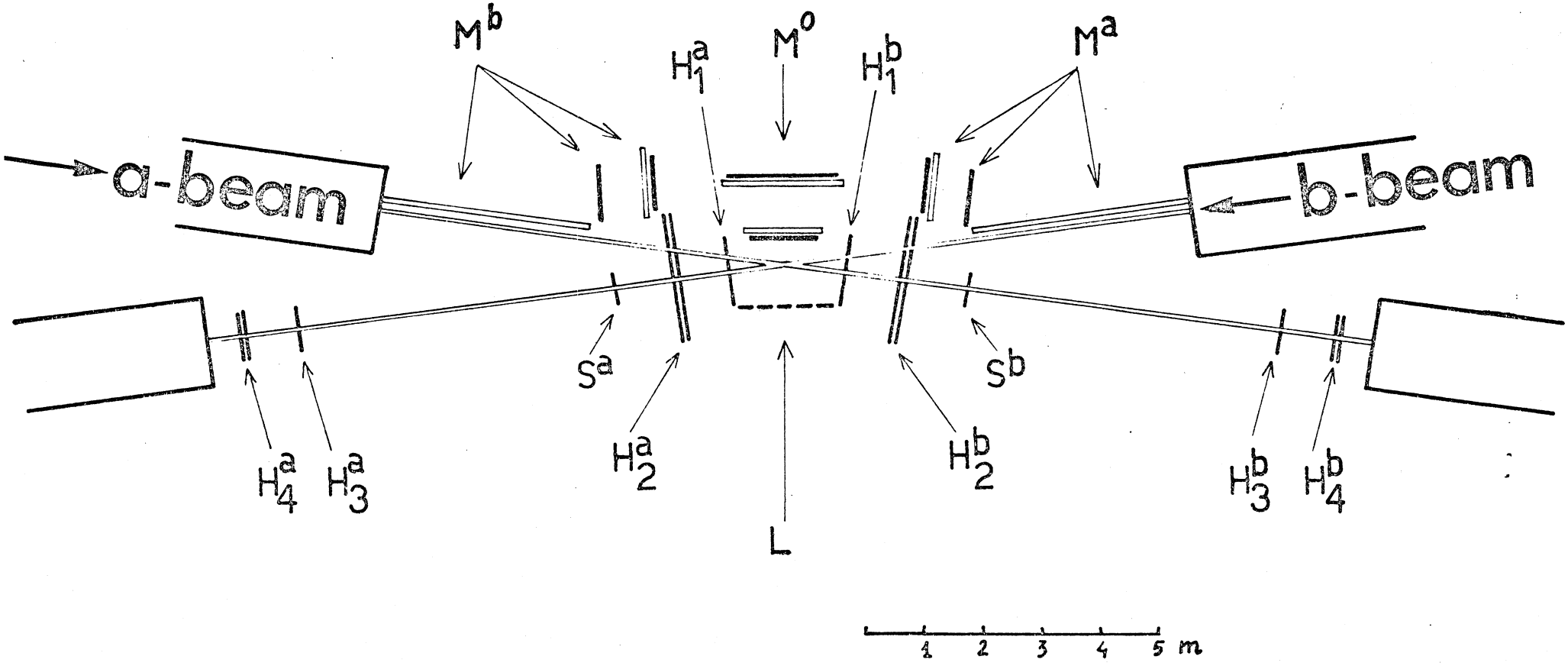

Fig. 2

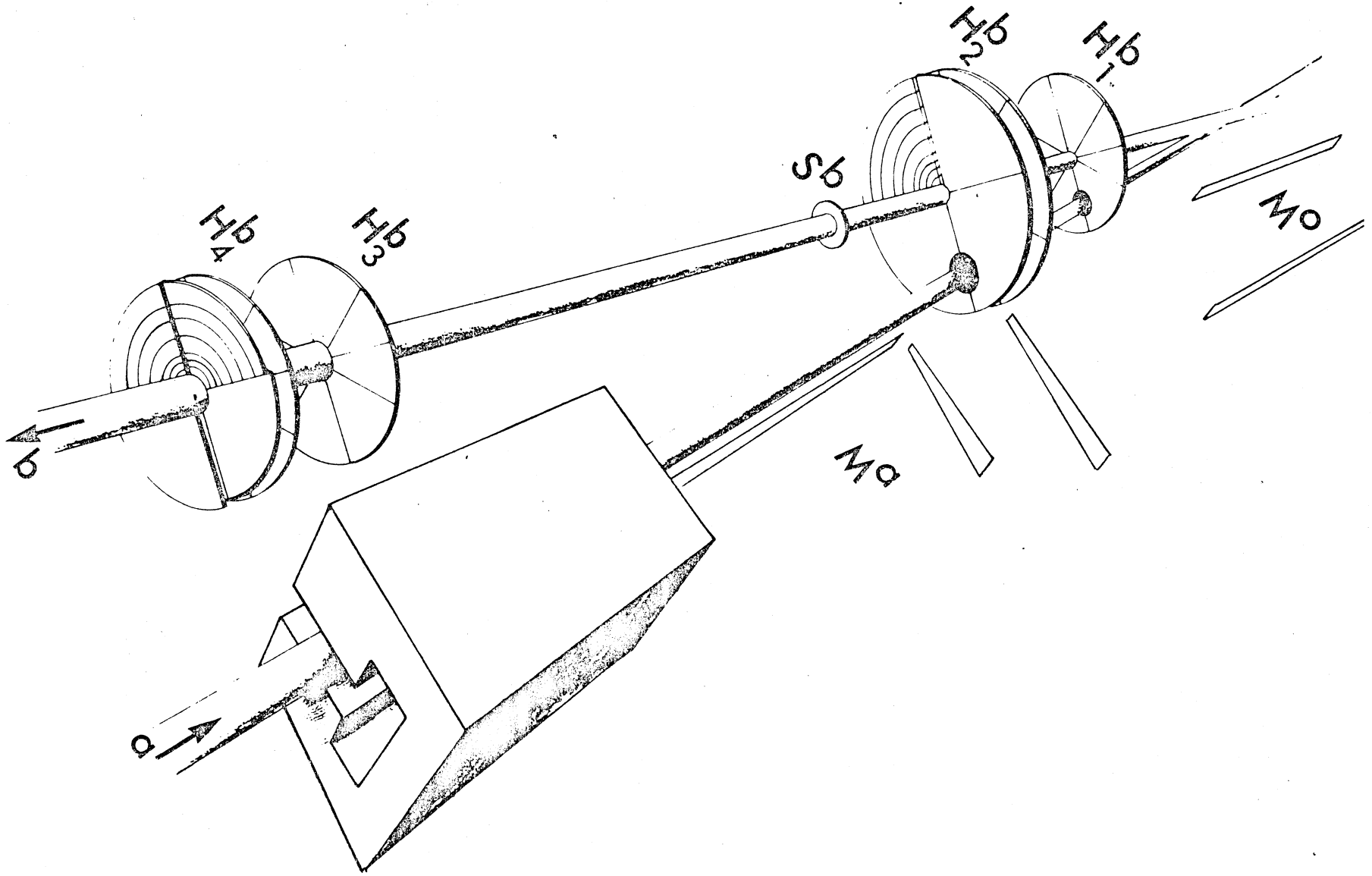

Fig. 3

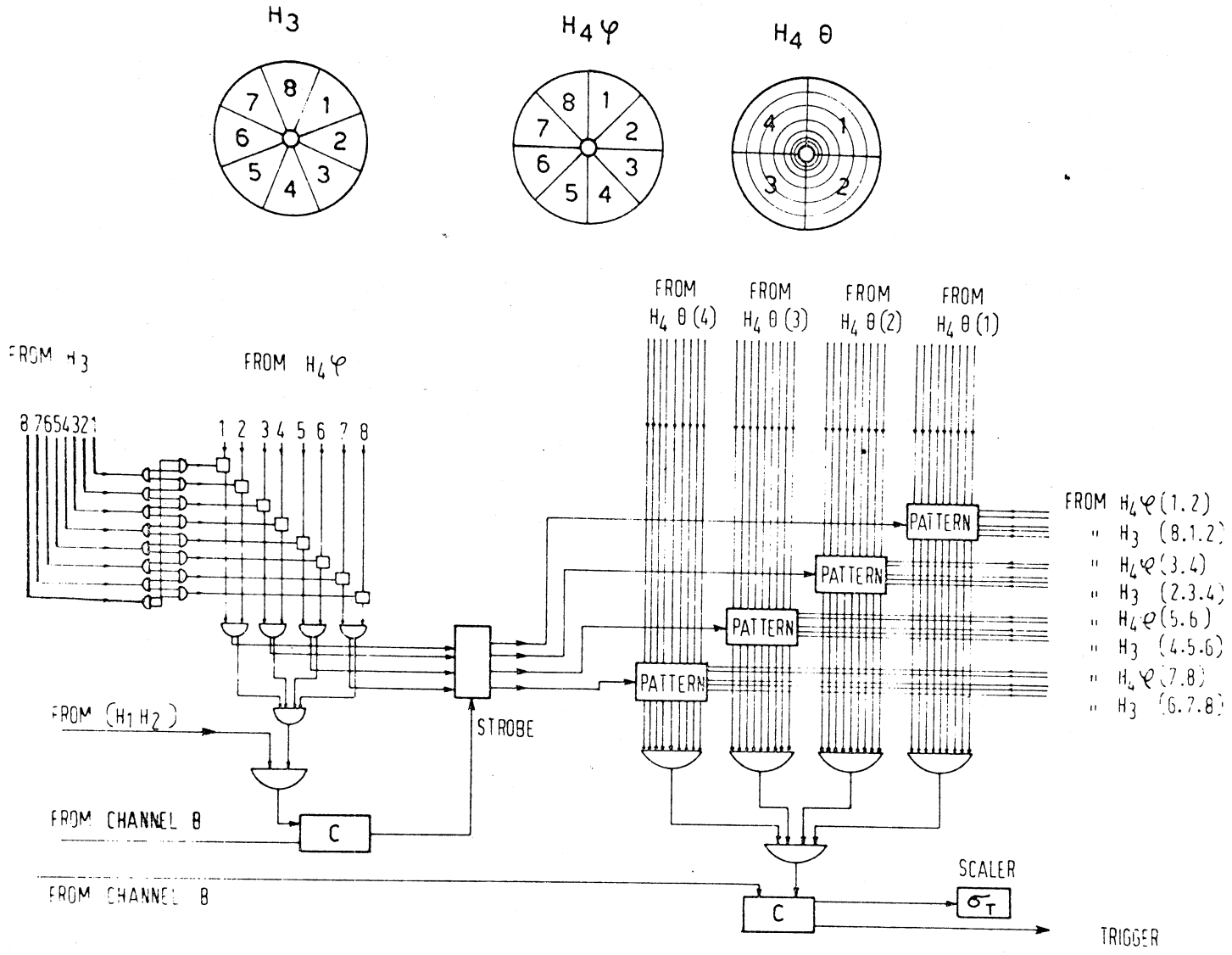
H3
H4 φ
H4 θ
FROM H3
FROM H4 φ
FROM H4 θ (4)
FROM H4 θ (3)
FROM H4 θ (2)
FROM H4 θ (1)
8 7 6 5 4 3 2 1
1 2 3 4 5 6 7 8
PATTERN
PATTERN
PATTERN
PATTERN
FROM H4 φ (1.2)
" H3 (8.1.2)
" H4 φ (3.4)
" H3 (2.3.4)
" H4 φ (5.6)
" H3 (4.5.6)
" H4 φ (7.8)
" H3 (6.7.8)
FROM (H1 H2)
STROBE
FROM CHANNEL 8
C
FROM CHANNEL 8
SCALER
C
TRIGGER

Fig. 4

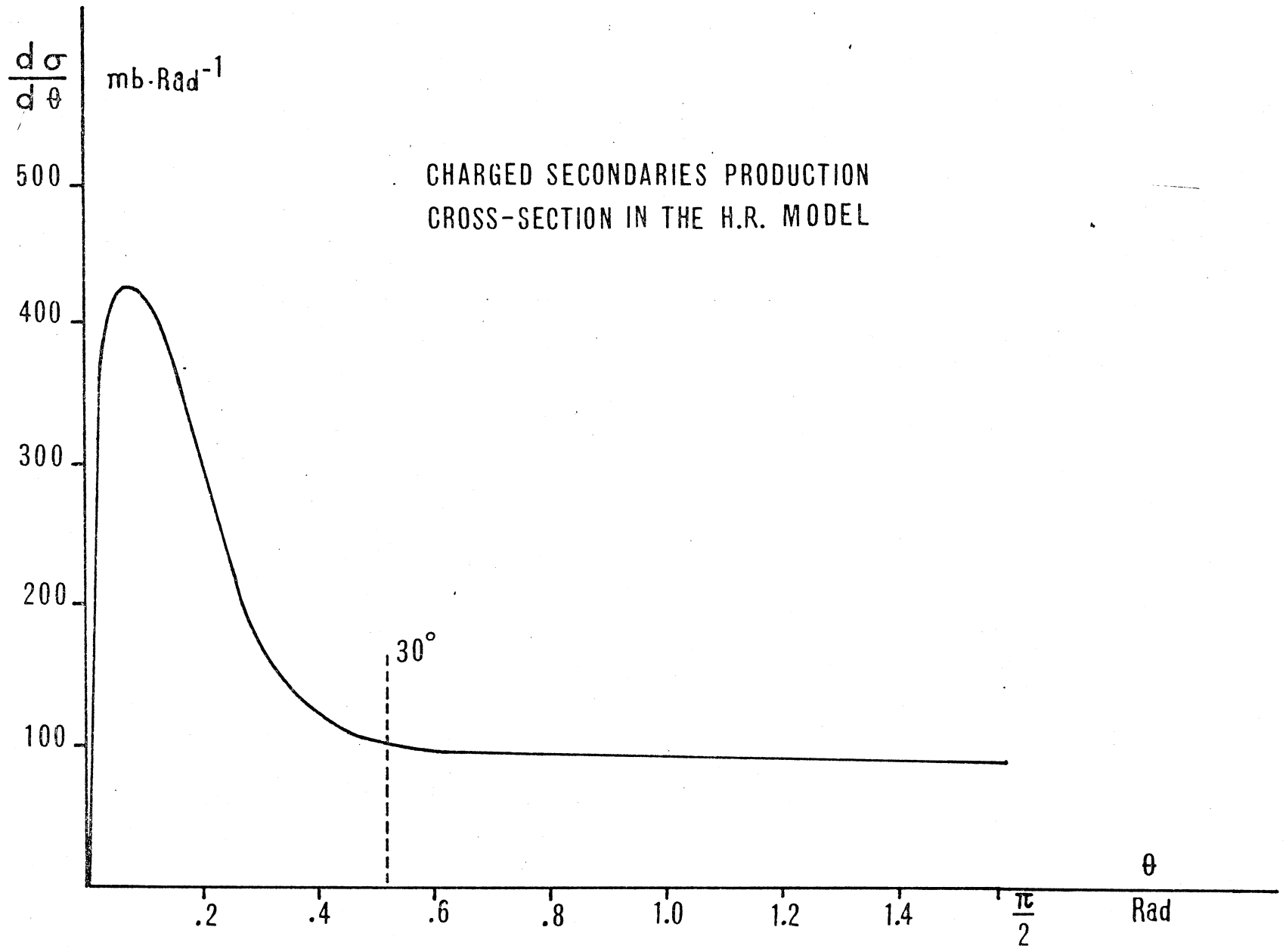
dσ/dθ
mb·Rad⁻¹
CHARGED SECONDARIES PRODUCTION
CROSS-SECTION IN THE H.R. MODEL
500
400
300
200
100
30°
.2
.4
.6
.8
1.0
1.2
1.4
π/2
θ
Rad

Fig. 5

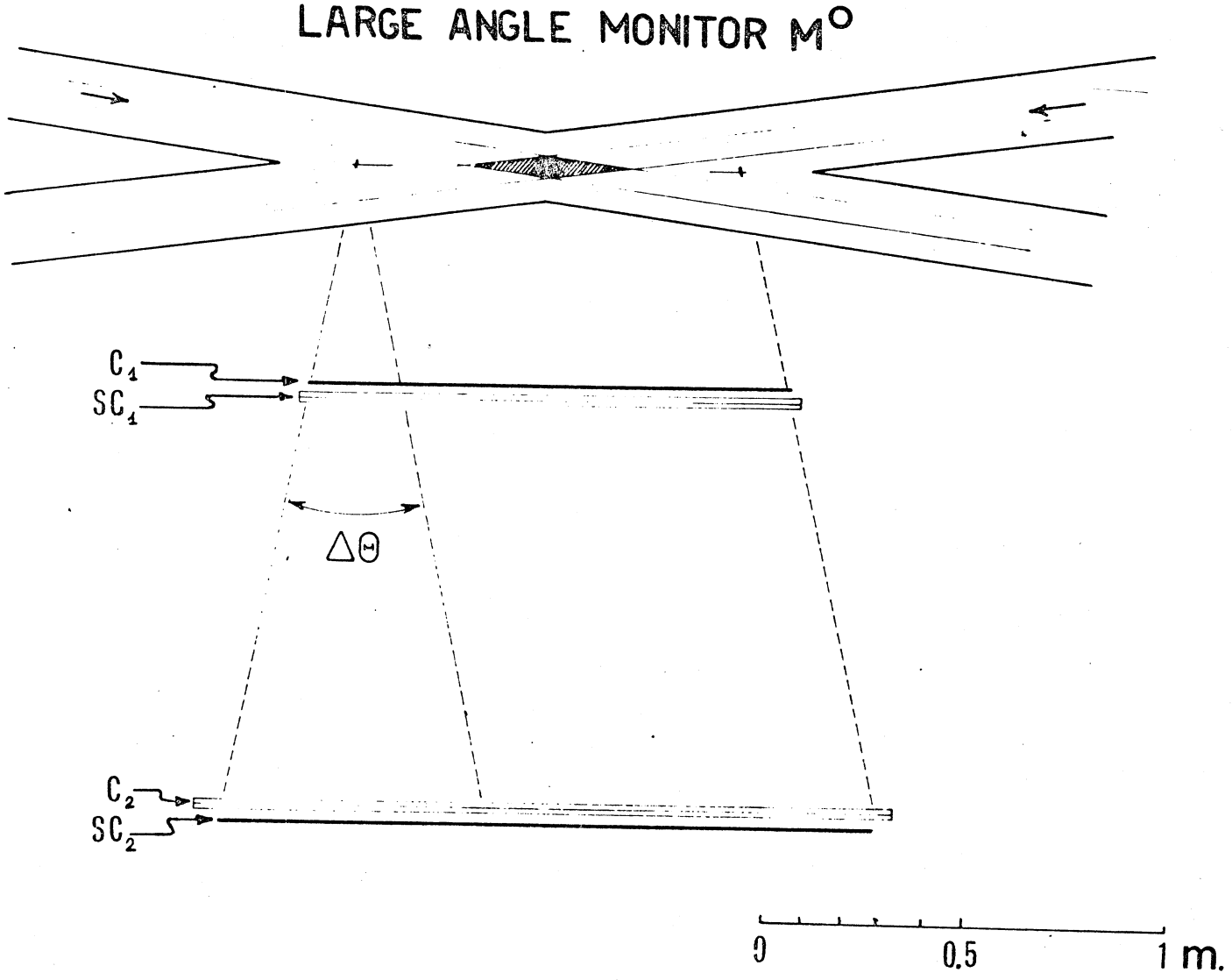

Fig. 7